



Article

LEO-Based Satellite Constellation for Moving Target Detection

Chongdi Duan ^{1,2,3}, Yu Li ^{3,*}, Weiwei Wang ³ and Jianguo Li ¹

¹ School of Information and Electronics, Beijing Institute of Technology, Beijing 100081, China; duancd@cast504.com (C.D.); jianguoli@bit.edu.cn (J.L.)

² National Key Laboratory of Science and Technology on Space Microwave, Xi'an 710100, China

³ Xi'an Institute of Space Radio Technology, Xi'an 710100, China; wangww83@cast504.com

* Correspondence: liy62@cast504.com

Abstract: With the rapid development of cooperative detection technology, target fusion detection with regard of LEO satellites can be realized by means of their diverse observation configurations. However, the existing constant false alarm ratio (CFAR) detection research rarely involves the space-based target fusion detection theory. In this paper, a novel multi-source fusion detection method based on LEO satellites is presented. Firstly, the pre-compensation function is constructed by employing the range and Doppler history of the cell where the antenna beam center is pointed. As a result, not only is the Doppler band broadening problem caused by the high-speed movement of the satellite platform, but the Doppler frequency rate (DFR) offset issue resulted from different observation configurations are alleviated synchronously. Then, the theoretical upper and lower limits of DFR are designed to achieve the effective clutter suppression and the accurate target echo fusion. Finally, the CFAR detection threshold based on the exponential weighted likelihood ratio is derived, which effectively increases the contrast ratio between the target cell and other background cells, and thus to provide an effective multi-source fusion detection method for LEO-based satellite constellation. Simulation results verify the effectiveness of the proposed algorithm.

Keywords: LEO; fusion detection; clutter suppression; doppler ambiguity; CFAR



Citation: Duan, C.; Li, Y.; Wang, W.; Li, J. LEO-Based Satellite Constellation for Moving Target Detection. *Remote Sens.* **2022**, *14*, 403. <https://doi.org/10.3390/rs14020403>

Academic Editor: Andrea Monti Guarnieri

Received: 2 November 2021

Accepted: 12 January 2022

Published: 16 January 2022

Publisher's Note: MDPI stays neutral with regard to jurisdictional claims in published maps and institutional affiliations.



Copyright: © 2022 by the authors. Licensee MDPI, Basel, Switzerland. This article is an open access article distributed under the terms and conditions of the Creative Commons Attribution (CC BY) license (<https://creativecommons.org/licenses/by/4.0/>).

1. Introduction

Spaceborne radar is confronted with low signal-to-noise ratio (SNR) problem in the long-distance detection process. For LEO-based satellite constellation, with the maturity of lightweight, standardized, low-cost development pattern as well as the rapid layout of different types of satellite echoes, i.e., communication, navigation and radar [1,2], multi-source fusion detection technology becomes a feasible means for reliable target detection, in which multi-station joint detection strategy is adopted to make full use of the advantage of multi-angle energy accumulation. The difficulty of related research lie in how to construct the multi-source fusion detection statistic and further improve the target detection performance.

Detection statistics are the key factors to CFAR performance, which are generally divided into the amplitude detection statistic [3] and the likelihood ratio detection statistic [4]. To address multi-source fusion detection issues, many relevant algorithms from different aspects have been discussed. The image reconstruction algorithm [5] is proposed by mining the correlation of oversampling signal between low resolution echo and high-resolution echo, in which the multi-resolution images are unified to the same resolution level, and thus the fusion detection performance degradation caused by resolution mismatch can be effectively avoided. The coherent CFAR detection algorithm [6] is developed by means of the orthogonal waveform to suppress clutter and interference. As a result, the target SNR and its corresponding CFAR detection performance can be improved. In literature [7], the spatial division algorithm under multi-source satellite configuration is demonstrated through constructing objective functions of distributed system, i.e., the path gain and the

positioning accuracy. In this way, the optimal spatial division criteria of key area can be achieved. Another type of typical method also referred as two-level threshold CFAR detection approach [8], is designed to solve the large data transmission problem for centralized detection system, where the local and global detection statistics are obtained by employing the primary threshold and the secondary threshold, respectively. On this basis, the analytical expressions of false alarm probability and detection probability are derived according to the multistage adaptive matched filter. For multiple platforms with different systematic error, the particle filter algorithm [9] is applied to compensate the measurement error and predict the adjacent target position based on the fused measurement information. Additionally, the target tracking accuracy can be significantly improved. Note that the first-order to third-order range migration can be simultaneously corrected by means of the symmetric keystone transform (SKT) without prior information, the multi-station fusion detection method [10] is presented by utilizing the space-ground asymmetric configuration in frequency modulation rate domain. In the aforementioned algorithms, the multi-source information fusion detection methods are realized in the image domain, and thus to improve the target SNR. However, it is difficult to fully exploit the multiple cell characteristics of the fused image, and hence results in the fusion detection performance degradation. To explore the enhanced CFAR detection method adapted to the multi-source fusion echoes, the core problem is how to mine the difference between the target cell and other background cells.

In this paper, a novel multi-source fusion detection method based on LEO satellites is proposed, where the basic idea is that multi-source echoes are combined to enhance target detection performance under the condition of LEO satellite platforms. The rest parts are outlined as follows. In Section 2, the theoretical model and the proposed method is discussed in detail, where the performance of pre-compensation process, clutter suppression and multi-source fusion CFAR detection are discussed. Numerical results are given in Section 3 to verify the effectiveness of the proposed method, and the corresponding advantages are comprehensively analyzed in Section 4. Finally, we draw a brief conclusion in Section 5.

2. Materials and Methods

Suppose that the observation scene is covered with multiple beams, each generated by a LEO-based satellite illuminator, as shown in Figure 1. Due to the distinct orbit parameters of different satellites, the echoes are concentrated over the dwell time and combined within an identical coordinate [11,12]. Accordingly, the enhanced multi-source fusion detection can be achieved.

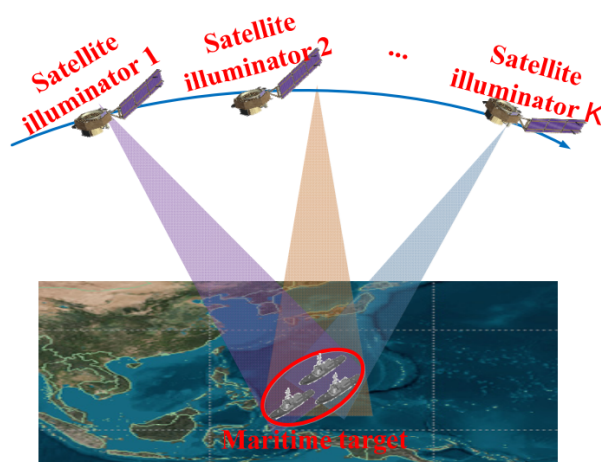


Figure 1. Multi-source fusion detection diagram.

For LEO satellites with different orbital velocity, moving direction and incident angle, there exists great differences in the range and Doppler history. This poses a considerable challenge for the robust fusion processing of multi-source echoes. Assume the echo of the k th satellite can be expressed as $S_k(R)$ in range domain, where $k = 1, 2, \dots, K$, R is the monostatic range, and K stands for the platform number. In terms of back projection (BP) operation, the surveillance area in rectangular coordinate is divided into several cells, and the monostatic range of each cell can be calculated by utilizing the observation configurations. Therefore, $S_k(R)$ can be represented as

$$R_k(x, y) = 2|\mathbf{P}_k(x, y, z) - \mathbf{P}_{Tg}(x, y, z_0)| \quad (1)$$

where $\mathbf{P}_k(x, y, z)$ and $\mathbf{P}_{Tg}(x, y, z_0)$ denote the satellite position vector and the target position vector, respectively, x, y, z are the corresponding coordinate value. To facilitate the subsequent processing, let the target locate on the earth's surface, and its rectangular coordinate is given by $\mathbf{P}(x, y, z_0) = (x, y, 0)$.

After the BP operation, $S_k(R)$ can be renewed as $S_k(x, y)$. According to the above projection relationship, the echoes with multiple satellites can be combined in the Cartesian coordinate $X - Y$. Here, the target signals corresponding to different satellites are presented as distinct iso-range lines, and the target position is located at the intersection of these iso-range lines. The multi-source fusion process [12] can be summarized as

$$S(x, y) = \frac{1}{K} \sum_k |S_k(x, y)| \quad (2)$$

2.1. Pre-Compensation of Spaceborne Echo for LEO Satellite

In literature [10], the moving target detection method is demonstrated with BeiDou satellites, in which the platform speeds are much lower than that of low orbit satellite, and the Doppler ambiguity problem can be ignored when integrating multiple echoes in DFR domain. However, this method is not applicable for the LEO constellation scenario. On one hand, the pulse repetition frequency (PRF) of the satellite illuminator is generally preset. Additionally, its adjustable dynamic range is limited. Thus, the high-speed movement of LEO satellites could apparently broaden the Doppler bandwidth (Bd) related to the observation scene and thus to reduce the target detectable interval, as indicated in Figure 2a. On the other hand, the extended Doppler bandwidth may exceed the given PRF, which leads to the Doppler ambiguity issue, as indicated in Figure 2b. In this case, the decoupling method, such as the KT transform [13], is no longer applicable owing to the Doppler ambiguity of the observation scene.

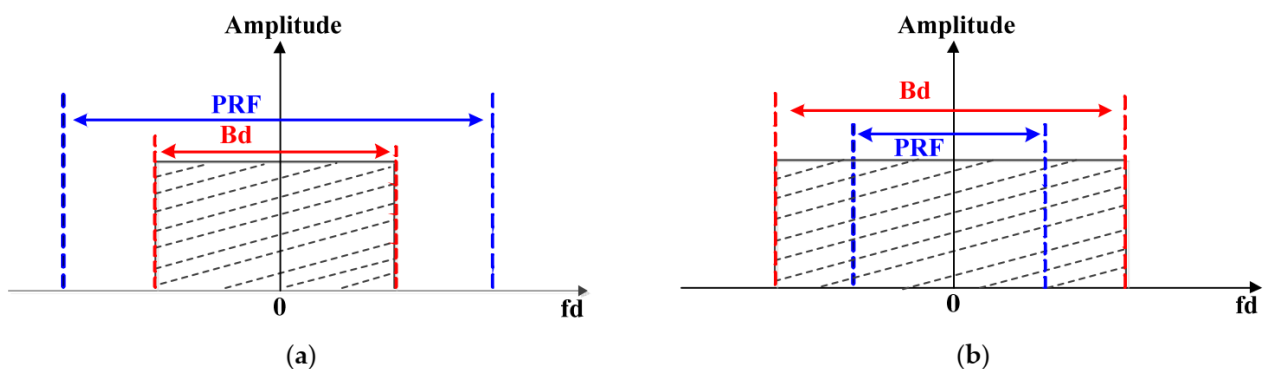


Figure 2. The relation between the extended Doppler bandwidth and the given PRF. (a) The limited target detectable interval as a result of the Doppler bandwidth expansion; (b) The Doppler ambiguity issue caused by the extended Doppler bandwidth.

On the other hand, the LEO satellites adopt the self-transmitting and self-receiving operation mode instead of the multiple-transmitting and single-receiving operation mode,

where the configuration does not possess the extreme asymmetry in respect of the GEO (Geostationary Orbit) or MEO (Medium Earth Orbit) satellites. Thus, the LEO-based multi-source echoes cannot be concentrated on one cell in DFR domain. For the multiple-transmitting and single-receiving operation mode, DFR of a moving target can be defined as [13]:

$$f_{dr1,k} = -\frac{1}{\lambda} \left\{ -|\mathbf{P}_{T,k} - \mathbf{P}_{Tg}|^{-3} \cdot [(\mathbf{P}_{T,k} - \mathbf{P}_{Tg})(\mathbf{v}_{T,k} - \mathbf{v}_{Tg})^T]^2 + |\mathbf{P}_{T,k} - \mathbf{P}_{Tg}|^{-1} \cdot (\mathbf{v}_{T,k} - \mathbf{v}_{Tg})^2 + |\mathbf{P}_{T,k} - \mathbf{P}_R|^{-3} \cdot [(\mathbf{P}_{T,k} - \mathbf{P}_R)(\mathbf{v}_{T,k} - \mathbf{v}_R)^T]^2 - |\mathbf{P}_{T,k} - \mathbf{P}_R|^{-1} \cdot (\mathbf{v}_{T,k} - \mathbf{v}_R)^2 - |\mathbf{P}_{Tg} - \mathbf{P}_R|^{-3} \cdot [(\mathbf{P}_{Tg} - \mathbf{P}_R)(\mathbf{v}_{Tg} - \mathbf{v}_R)^T]^2 + |\mathbf{P}_{Tg} - \mathbf{P}_R|^{-1} \cdot (\mathbf{v}_{Tg} - \mathbf{v}_R)^2 \right\} \quad (3)$$

While that of the self-transmitting and self-receiving operation mode is given by:

$$f_{dr2,k} = -\frac{2}{\lambda} \left\{ -|\mathbf{P}_{T,k} - \mathbf{P}_{Tg}|^{-3} \cdot [(\mathbf{P}_{T,k} - \mathbf{P}_{Tg})(\mathbf{v}_{T,k} - \mathbf{v}_{Tg})^T]^2 + |\mathbf{P}_{T,k} - \mathbf{P}_{Tg}|^{-1} \cdot (\mathbf{v}_{T,k} - \mathbf{v}_{Tg})^2 \right\} \quad (4)$$

In Equations (3) and (4), λ is the wavelength, $\mathbf{P}_{T,k}$ and \mathbf{P}_R stand for the position vector of the k th transmitting platform and the receiving platform, respectively. $\mathbf{v}_{T,k}$ and \mathbf{v}_R denote the corresponding velocity vector in turn. \mathbf{P}_{Tg} and \mathbf{v}_{Tg} are the position vector and the velocity vector of the target.

Under the condition of bistatic configuration with GEO or MEO satellite as its transmitter, Equation (3) can be approximately expressed as:

$$f_{dr1,k} \approx -\frac{1}{\lambda} \left\{ -|\mathbf{P}_{Tg} - \mathbf{P}_R|^{-3} \cdot [(\mathbf{P}_{Tg} - \mathbf{P}_R)(\mathbf{v}_{Tg} - \mathbf{v}_R)^T]^2 + |\mathbf{P}_{Tg} - \mathbf{P}_R|^{-1} \cdot (\mathbf{v}_{Tg} - \mathbf{v}_R)^2 \right\} \quad (5)$$

From Equation (5), the target DFR mainly depends on the position vector of the receiving platform under asymmetric configuration. Therefore, the multiple-transmitting and single-receiving operation mode is conducive to the fusion processing [10]. However, the echoes related to multiple satellites cannot be directly integrated due to the distinct orbit parameters in respect of the self-transmitting and self-receiving operation mode, and the approximate Equation (4) is not valid here. To realize the universality of the multi-source fusion detection in respect of LEO-based satellite constellation, the robust fusion detection method should be presented to meet the application requirements of communication, navigation and radar with different orbital altitudes. In this section, the pre-compensation method of multi-source echoes is introduced based on the prior information, i.e., high-speed motion characteristic and spaceborne observation configuration.

By applying the Fast Fourier Transform (FFT) operation to the range-compressed signal, the echo of the k th satellite can be expressed as:

$$S_k(f_\tau, \eta) = \sigma_\eta P(f_\tau) \text{rect}\left(\frac{\eta}{T_a}\right) \exp[-j2\pi \frac{f_\tau + f_c}{c} R_k(\eta)] \quad (6)$$

where f_τ and η represents the fast-frequency and slow-time, T_a is the dwell time, f_c is the carrier frequency. $P(f_\tau)$ denotes the Fourier transform of the range envelope. $R_k(\eta)$ stands for the monostatic range of the k th satellite.

Since the ephemeris and the antenna beam directivity of each satellite are known, the pre-compensation of the whole observation scene can be carried out according to the range and Doppler history of the cell where the beam center is pointed. The pre compensation function is given by:

$$H_k(f_\tau, \eta) = \exp[-j2\pi \frac{f_\tau + f_c}{c} R_k(\eta)] \quad (7)$$

Based on the above pre-compensation operation, the Doppler band broadening caused by the high-speed motion platform as well as the DFR offset resulted from the observation configuration can be effectively alleviated.

2.2. Clutter Suppression Based on DFR Design

In view of the aforementioned pre-compensation strategy, the multi-source fusion process is performed in this section through setting the cell interval in DFR domain. On one hand, for the LEO-based satellites with different orbit elements and incident angles, although the DFR difference of clutter echoes can be corrected by employing the range and Doppler history of the cell where the beam center is pointed, the target velocity vector may still cause the dispersion of the target fusion energy in DFR domain. Therefore, there exists a theoretical lower bound for the DFR cell, where the multi-source echoes can be entirely integrated in the same cell. On the other hand, for the sake of the resolving ability in DFR domain, the echoes related to the target and the observation scene should be separated with an interval greater than the DFR cell, which possesses a theoretical upper bound accordingly.

Multiplying $S_k(f_\tau, \eta)$ by $H_k(f_\tau, \eta)$, the compensated signal in range-DFR domain [10] can be represented as $S'_k(R, f_{dr})$. Let the cell size of DFR be $\Delta_{f_{dr}}$, and the parameter selection technique of $\Delta_{f_{dr}}$ should meet the following restrictions to achieve accurate information fusion as well as the effective clutter suppression.

(i) The DFR deviation of the target between any two satellites should be less than $\Delta_{f_{dr}}/2$, that is,

$$|f_{dr2,m} - f_{dr2,n}| < \Delta_{f_{dr}}/2 \quad (8)$$

In Equation (8), $f_{dr2,m}$ and $f_{dr2,n}$ are DFRs of the m th satellite and the n th satellite, respectively. m and n satisfy $1 \leq m, n \leq K, m \neq n$. According to Equation (4), Equation (8) can be described as:

$$\left| \frac{2}{\lambda} \{ |\mathbf{P}_{T,m} - \mathbf{P}_{Tg}|^{-3} \cdot [(\mathbf{P}_{T,m} - \mathbf{P}_{Tg})(\mathbf{v}_{T,m} - \mathbf{v}_{Tg})^T]^2 - |\mathbf{P}_{T,n} - \mathbf{P}_{Tg}|^{-3} \cdot [(\mathbf{P}_{T,n} - \mathbf{P}_{Tg})(\mathbf{v}_{T,n} - \mathbf{v}_{Tg})^T]^2 \right. \\ \left. - |\mathbf{P}_{T,m} - \mathbf{P}_{Tg}|^{-1} \cdot (\mathbf{v}_{T,m} - \mathbf{v}_{Tg})^2 + |\mathbf{P}_{T,n} - \mathbf{P}_{Tg}|^{-1} \cdot (\mathbf{v}_{T,n} - \mathbf{v}_{Tg})^2 \right| < \frac{\Delta_{f_{dr}}}{2} \quad (9)$$

where $\mathbf{P}_{T,m}$ and $\mathbf{P}_{T,n}$ stand for the position vectors of the m th satellite and the n th satellite. $\mathbf{v}_{T,m}$ and $\mathbf{v}_{T,n}$ denote the corresponding velocity vector.

(ii) The DFR deviation between the target and the observation scene should be greater than $\Delta_{f_{dr}}$, namely,

$$|f_{dr2,k} - f_{dr2,clutter,k}| > \Delta_{f_{dr}} \quad (10)$$

where $f_{dr2,k}$ and $f_{dr2,clutter,k}$ represent DFRs corresponding to the target and the clutter in turn.

Combined with the aforementioned constraint conditions, the optional interval of $\Delta_{f_{dr}}$ can be obtained.

2.3. Multi-Source Fusion CFAR Detection with LEO-Based Satellite Constellation

The accurate target echo focusing as well as the effective clutter suppression can be realized based on the above pre-compensation process and cell interval setting strategy. However, the direct CFAR detection procedure could result in the deterioration of target detection performance due to the target detection range difference with regard of multi-source satellites. In this section, the echo fusion and target detection processes are performed in the ENU (East North Up) coordinate through employing the coordinate system transformation operation. The main steps of multi-source fusion CFAR detection method are given below.

Step 1 Multi-source fusion of target echoes.

By performing the focusing operation in range-DFR domain, the K groups of echoes $S'_k(R, f_{dr0})$ from multiple satellites can be obtained in terms of their observation configurations, in which f_{dr0} denotes the cell position where the target is located, and $k = 1, 2, \dots, K$. Then, $S'_k(R, f_{dr0})$ can be reformulated as $S''_k(x, y)$ through transforming the fused data from range coordinate to Cartesian coordinate. In this way, the multi-station echo fusion process can be completed by means of incoherent integration, as presented in Equation (2), and the multi-source fusion echo can be expressed as:

$$S''(x, y) = \frac{1}{K} \sum_{k=1}^K |S_k''(x, y)| \quad (11)$$

Step 2 Weight calculation of the contrast ratio based on the sliding window.

Assume that the sliding window is composed of $M \times M$ cells, in which the central position is represented as (x_0, y_0) , and the edge region is described as $(x_0 + i, y_0 + j)$. The weight of the contrast ratio in respect of the sliding window center is indicated by:

$$\eta(x_0, y_0) = \frac{|S''(x_0, y_0)|}{\sum_{i,j} |S''(x_0 + i, y_0 + j)|} \quad (12)$$

where i and j satisfy $i, j = -\text{floor}(\frac{M-1}{2}), \dots, -1, 0, 1, \dots, -\text{floor}(\frac{M-1}{2}), i, j \neq 0$, floor denotes the round down operation.

Step 3 Exponential weighted likelihood ratio modeling.

The exponential weighted likelihood ratio is given by:

$$\text{Ratio}(x, y) = \log_e \left[\frac{p(z(x, y)|H_1)}{p(z(x, y)|H_0)} \eta(x, y) \right] \quad (13)$$

where the natural constant e is set to 2.71828. $z(x, y)$ is the measured value of (x, y) after exponential operation, namely, $z(x, y) = \exp(S(x, y))$, where \exp stand for the exponential operation. $p(z(x, y)|H_1)$ and $p(z(x, y)|H_0)$ are the probability density functions corresponding to the cases that the target does or does not exist. That is,

$$p(z(x, y)|H_1) = \frac{1}{\sqrt{2\pi}\sigma} \exp\left[-\frac{(z(x, y) - A)^2}{2\sigma^2}\right] \quad (14)$$

$$p(z(x, y)|H_0) = \frac{1}{\sqrt{2\pi}\sigma} \exp\left[-\frac{z(x, y)^2}{2\sigma^2}\right] \quad (15)$$

As can be seen from Equation (14), the probability density functions become smaller as the cell under test gets farther from the target, where A and σ are the target amplitude and the noise standard deviation. Here, the likelihood ratio detection statistic [4] is more suitable for target fusion detection as a result of its joint detection property, compared with the amplitude detection statistic [3]. That is, the amplitudes of the target cell and other background cells are directly employed to acquire a detection threshold when constructing the amplitude detection statistic. Hence, the former is employed to construct the multi-source fusion detection factor in this paper.

Step 4 Multi-source fusion CFAR detection.

The selection method of CFAR threshold [14] T_0 is given by

$$T_0 = \frac{(2I - 2)/(I - 2) - 1}{(P_{fa})^{[(I-2)/(2I-2)]}} + 1 - \frac{(2I - 2)}{(I - 2)} \quad (16)$$

where I is the second-order statistics of the exponential weighted likelihood ratio. P_{fa} represents the false alarm probability. Here, the difference between CA-CFAR method [3] and the proposed method are chiefly as follows. For CA-CFAR method, the amplitudes of the target cell and other background cells are directly employed to acquire a threshold, which is suitable for point target detection. That is, the target occupies only one cell in the sliding window. While the presented detection method is applicable to distributed target detection, whose energy is located in distinct iso-range lines after the multi-source fusion process. In this case, the contrast ratio between the target cell and other background cells could be effectively enhanced in terms of the exponential weighted likelihood ratio.

Figure 3 demonstrates the flow chart of multi-source fusion CFAR detection algorithm with regard of the LEO-based satellite constellation.

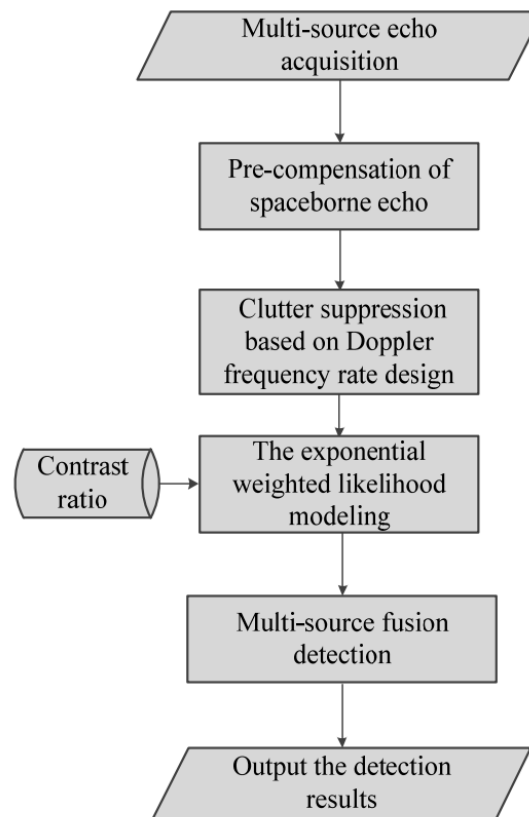


Figure 3. The flow chart of multi-source fusion CFAR detection algorithm.

3. Results

To illustrate the effectiveness of the proposed method with LEO-based satellite constellation, it is necessary to consider the impact of terrain and sea clutter on moving target detection under down looking mode, that is, the signal-to-clutter ratio (SCR) problem. Furthermore, the influence of fusion energy dispersion on moving target detection caused by the high-speed motion of LEO satellites should also be taken into account, that is, the SNR problem. Thus, the performance of the presented method is evaluated comprehensively from three aspects, i.e., pre-compensation, clutter suppression and multi-source fusion detection. Considering that there is no published real measured data for LEO satellite scenario, without loss of generality, the simulation results of multi-source echoes are generated to evaluate the performance of the proposed algorithm.

3.1. Pre-Compensation Results

Figure 4 shows the SKT [10] processing results of the LEO-based satellite echo before and after the pre-compensation operation. It can be seen from Figure 4a that there exists obvious range cell migration (RCM) in the original echo. For LEO satellite, the severe Doppler ambiguity issue will lead to the mismatch of SKT compensation function, and the first-order to third-order RCM cannot be removed, as indicated in Figure 4b. While the Doppler ambiguity issue can be solved by implementing the pre-compensation operation. Besides, the range-azimuth coupling problem is correctly handled after SKT process, as demonstrated in Figure 4c. Here, the orbit eccentricity, orbit height, rising intersection right ascension, orbit inclination, perigee angle, perigee time, azimuth and pitch angle of the antenna beam center related to the satellite is set to 0.003, 580 km, 195°, 55°, 200°, 0, 90° and 30°, respectively. For each satellite, the PRF, carrier frequency and signal bandwidth

are given by 1000 Hz, 9.65 GHz and 50 M. Let the intersection point of the beam center and the earth surface be the coordinate origin, and the moving target coordinate is given by [5 km, 1 km].

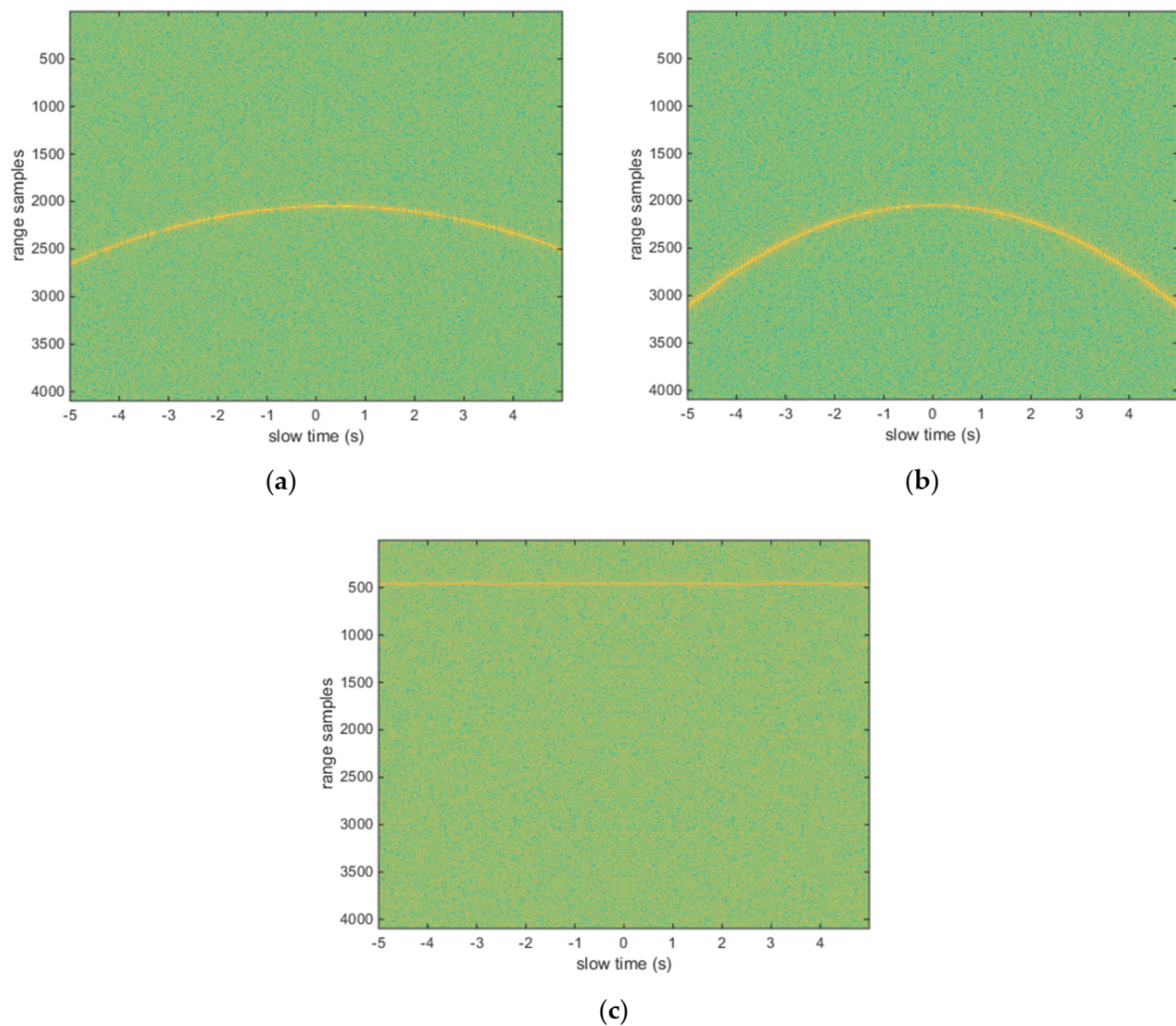


Figure 4. SKT processing results before and after the pre-compensation operation. (a) The original echo; (b) SKT processing results before the pre-compensation operation; (c) SKT processing results after the pre-compensation operation.

Based on the above pre-compensation operation, the multi-source fusion result in range-DFR domain is shown in Figure 5, where the satellite number is 4, and the parameter setting is consistent with that in the upper paragraph, except that the perigee times of the other three satellites are set as $[-0.5, 0.5, -1.5]$. Here, the perigee time is defined as the moment when a satellite is nearest the earth, around which it turns, and the perigee time in this paper is measured in seconds.

For the pre-compensation operation, it should be noted that the echoes over the 10 s dwell time are segmented into 5 frames as a result of the complex reflectivity fluctuation, and the complex reflectivity can be regarded as a constant within each frame. That is, coherent accumulation is performed within one frame, and incoherent accumulation is carried out between two adjacent frames.

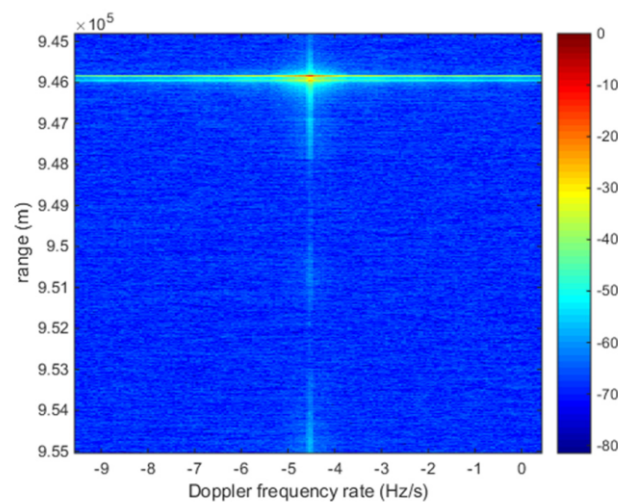


Figure 5. The multi-source fusion result with LEO-based satellite constellation.

To evaluate the theoretical boundary of the pre-compensation operation, Figure 6 shows the unambiguous Doppler interval, as revealed in the yellow area, which is depending on the target velocity vector as well as the range between the cell where the beam center is pointed and that is under test. In ENU coordinate, the included angle of the target velocity direction is set as 45 degrees along the x axis in clockwise direction. One can see that there exists no Doppler ambiguity issue provided that the target velocity is less than 63 knots, and the range deviation from the cell where the beam center is pointed is within a 80 km radius.

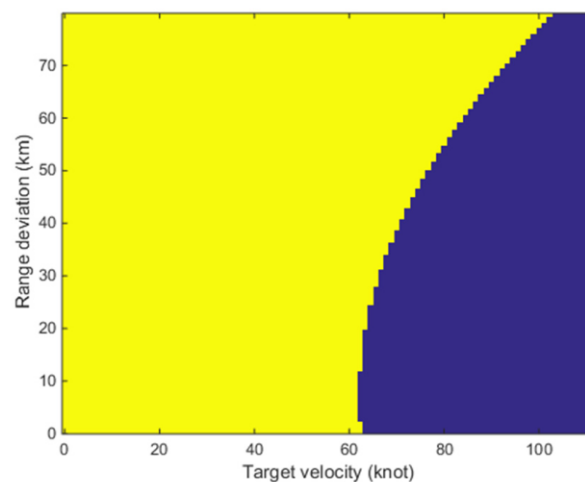


Figure 6. The unambiguous Doppler interval.

3.2. Clutter Suppression Results

The theoretical upper limit and lower limit of DFR is discussed in Section 2.2, in which the former requires that the echoes related to the target and the clutter can be separated in DFR domain. Figure 7a,b illustrates the distribution results of the target and that of the clutter, respectively. Here, only the clutter corresponding to the antenna main lobe is considered when setting the DFR interval, and the main lobe beamwidths along the pitch direction and the azimuth direction are set to 6 degrees and 9 degrees in turn. The target velocity is 20 knots, and its direction deviates from the x axis by 45 degrees in the clockwise direction.

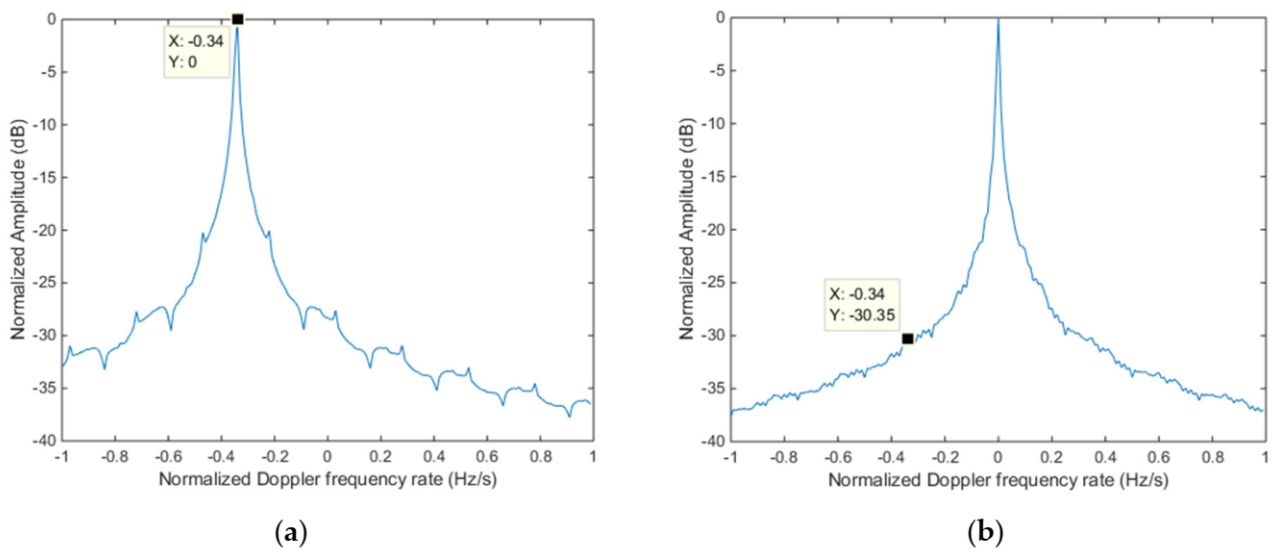


Figure 7. The distribution results of the target and the clutter. (a) The target echo in DFR domain; (b) The clutter echo in DFR domain.

While the latter requires that the multi-source echoes can be integrated to the same cell, Figure 8 illustrates the relationship between the target velocity and the optional interval of Δf_{dr} , in which the optional interval of Δf_{dr} is located between the dotted line and the solid line, and the constraint interval of Δf_{dr} gradually relaxes with the increase of the target velocity.

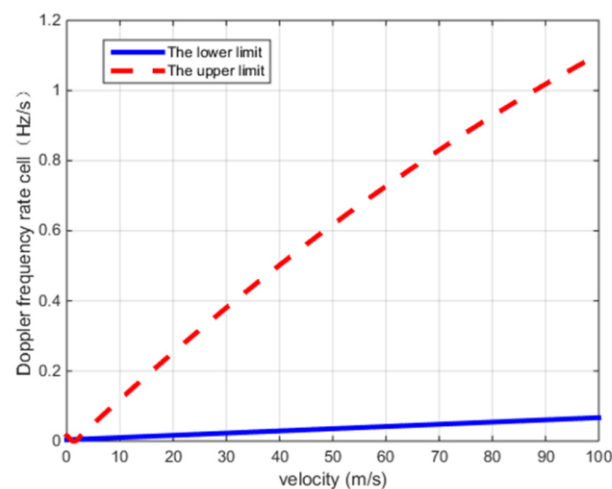


Figure 8. The relationship between the target velocity and the optional cell interval in DFR domain.

3.3. Multi-Source Fusion CFAR Detection Results

The three-dimensional projection results from range-DFR domain $R - f_{dr}$ to Cartesian-DFR domain $X - Y - f_{dr}$ after multi-source fusion is demonstrated in Figure 9a. To evaluate the performance of the proposed method in detail, the slice of the fusion results along DFR bins is given in Figure 9b. Compared with Figure 9a, the noise power in Figure 9b will decrease. Assume there are K DFR bins in Figure 9a, and the noise power in Figure 9b is $\frac{1}{K}$ that of Figure 9a due to the noise power accumulated along DFR bins with incoherent accumulation mode. One can see that the echoes with multiple satellites are focused on the same cell, which agrees with the theoretical analysis. Considering the target fluctuation characteristics caused by the diverse incident angles of multiple satellites, 3 dB amplitude fluctuation is added to the multi-source echoes in the simulation process, other simulation parameters are consistent with that in Section 3.1.

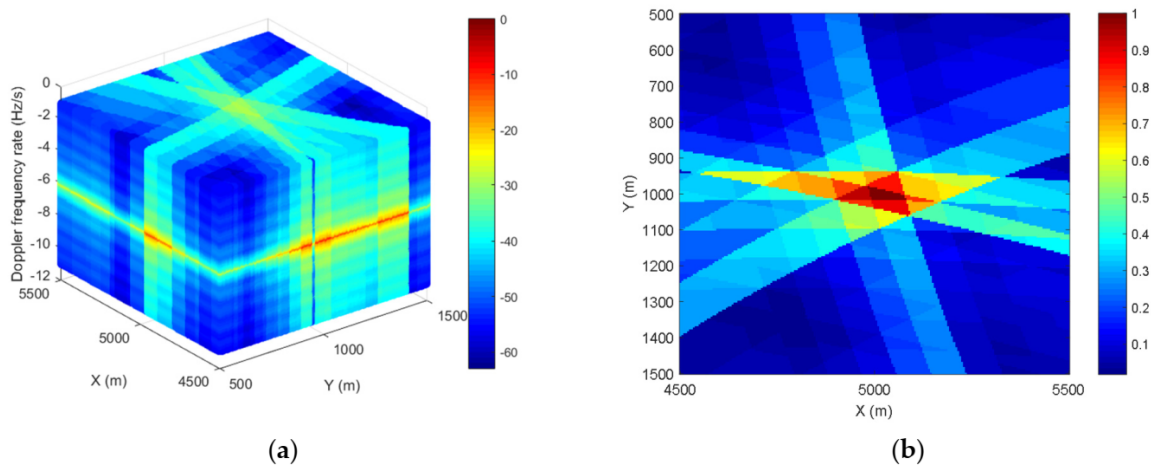


Figure 9. The multi-source fusion results of the target echo. (a) The target fusion result in Cartesian-DFR domain; (b) The slice of the fusion result along DFR bins.

Assume that the sliding window is composed of 3×3 cells, Figure 10a shows the weight distribution of the contrast ratio based on the sliding window, where the diffusion energy around the target cell is greatly decreased through introducing the contrast between the sliding window center and the edge region. Figure 10b reveals the exponential weighted likelihood ratio distribution corresponding to the fusion result. Compared with the likelihood ratio, the exponential weighted likelihood ratio increases the contrast between the target cell and the adjacent cells, which is conducive to improve the multi-source fusion CFAR detection algorithm.

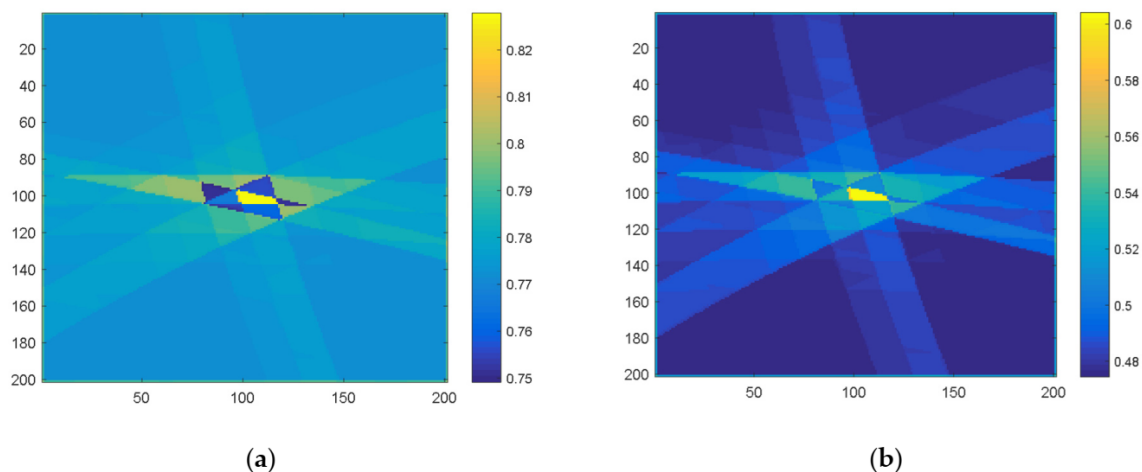


Figure 10. The intermediate variables in the multi-source fusion process. (a) The weight distribution of the contrast ratio based on the sliding window; (b) The exponential weighted likelihood ratio distribution corresponding to the fusion result.

Suppose that the target fluctuation type follows Swerling I distribution [15], the performance corresponding to different likelihood ratio based (LRB) detection methods [4] is compared in Figure 11a, where the false alarm probability is set to 1×10^{-6} , Monte Carlo simulation times is 500, and the SNR interval is set to 3~15 dB. One can see that the LRB detection method with multiple platforms could effectively enhance the detection probability, compared with LRB detection method with a single platform. Accordingly, the effectiveness of the multi-source fusion theory can be verified. While the proposed likelihood ratio weighting based (LRWB) detection method with multiple platforms could further improve the detection performance, especially for low target SNR interval. The

fusion CFAR detection results with different methods are indicated in Figure 11b–d under the condition that the false alarm probability is 1×10^{-6} and SNR is 7 dB, among which the target region can be extracted more precisely by means of the LRWB method.

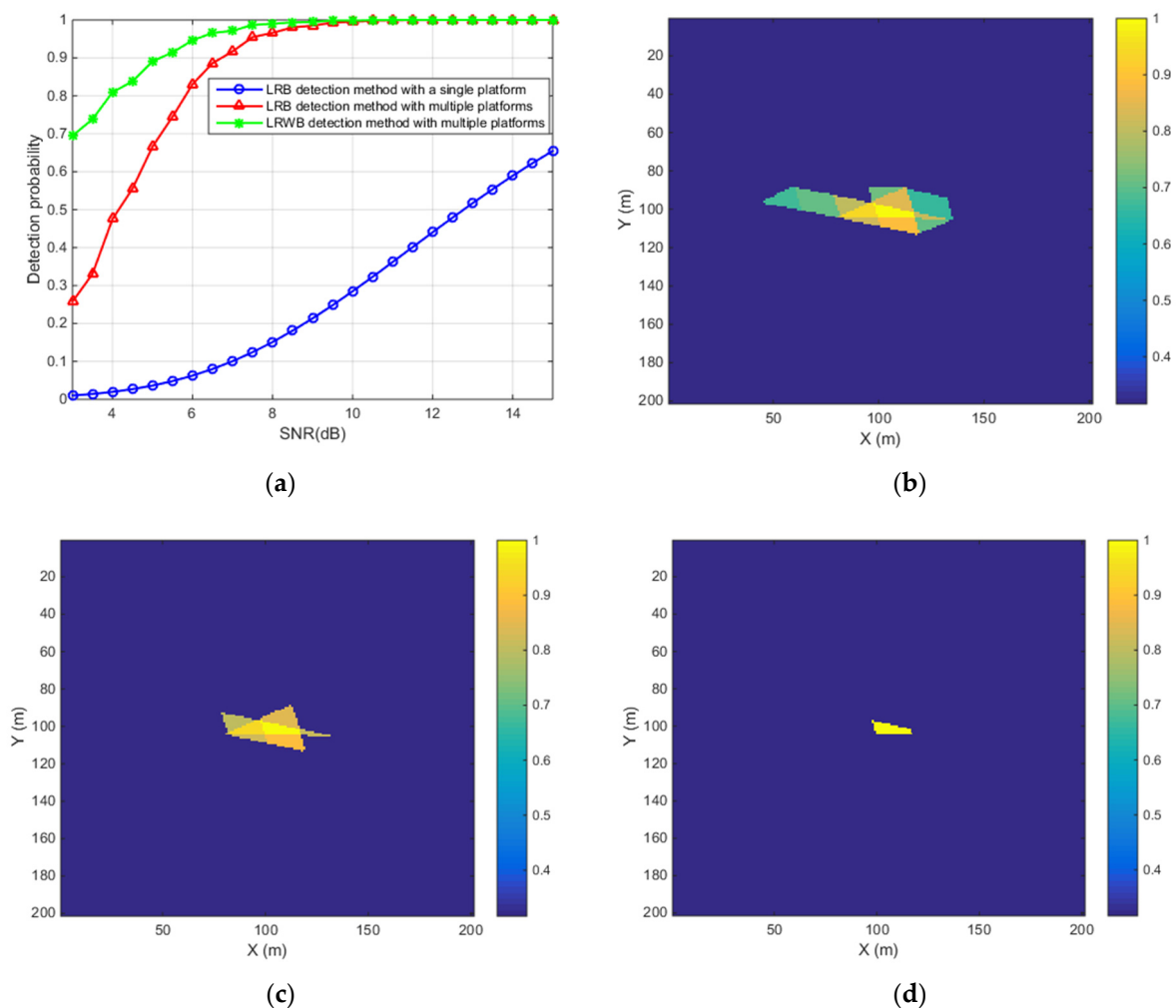


Figure 11. Detection performance analysis. (a) The detection probability with different methods; (b) The detection result using LRB detection method with a single platform; (c) The detection result using LRB detection method with multiple platforms; (d) The detection result using LRWB detection method with multiple platforms.

For multiple targets scenario, multi-source fusion results are demonstrated in Figure 12, where the two moving target coordinates are given by $[-0.5 \text{ km}, 1.5 \text{ km}]$ and $[4 \text{ km}, 2 \text{ km}]$ respectively, and other parameters are consistent with the former. Figure 12a shows the multi-source fusion result. From Figure 12b,c, both the weight distribution and the exponential weighted likelihood ratio distribution reveal that the diffusion energy around the two target cells is greatly decreased. The comparison results with different methods are given in Figure 12d–f, and one can see that the two target regions can be extracted more precisely by means of LRWB method, which further verify the effectiveness of our theoretical analysis.

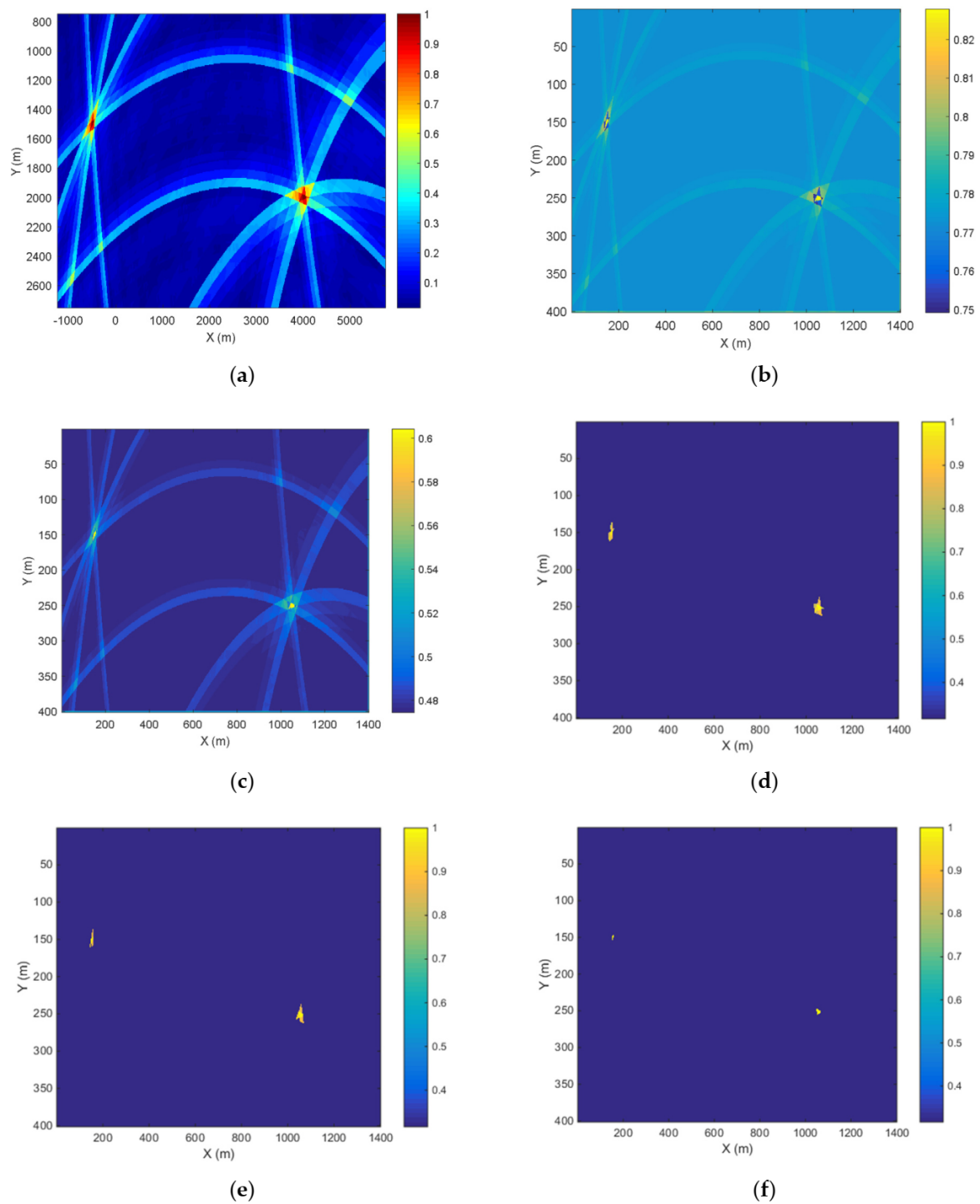


Figure 12. Multi-source fusion results with regard to multiple targets scenario. (a) Multi-source fusion result; (b) The weight distribution of the contrast ratio based on the sliding window; (c) The exponential weighted likelihood ratio distribution corresponding to the fusion result; (d) The detection result using LRB detection method with a single platform; (e) The detection result using LRB detection method with multiple platforms; (f) The detection result using LRWB detection method with multiple platforms.

In conclusion, the LRWB detection method based on the exponential weighted likelihood ratio could effectively improve the target detection performance with multi-source platforms.

4. Discussion

A novel multi-source fusion detection method based on LEO satellites has been introduced in this paper. The application of pre-compensation, clutter suppression and multi-source fusion detection processes demonstrates the efficiency of our study in moving target detection process.

Considering that LEO-based satellite constellation is confronted with the non-coincidence problem with regard of multi-source echoes. That is, the target focusing positions with different LEO satellites do not coincide at one cell in DFR domain as a result of the high-speed motion platform, which can be solved by constructing the pre-compensation function based on the antenna beam directivity. From Figure 5, one can see that the target energy can be focused on the same cell in DFR domain after multi-source fusion process, which further verifies the effectiveness of our pre-compensation theory.

For the DFR-based clutter suppression strategy, the size of the DFR cell is designed by deducing its upper and lower limits according to the multi-station configuration. In this way, both the clutter suppression effectiveness and the multi-station fusion efficiency are taken into consideration. For the DFR cell where the target is located, the corresponding clutter echo can be suppressed more than 30 dB through reasonably setting the maximum value of DFR cell, as indicated in Figure 7a,b. In Figure 8, the target echo fusion problem caused by high-speed motion platform can be greatly alleviated by selecting the minimum value of the DFR cell.

Further, the enhanced CFAR detection strategy based on the exponential weighted likelihood measurement can be carried out by transforming the fused data from range coordinate to Cartesian coordinate, which essentially reduces the false alarm probability caused by the echo fusion related to different range loops in multi-station configuration. For the first step, the echo fusion process is performed through employing the coordinate system transformation operation, and the echoes with multiple satellites are focused on the same cell, as demonstrated in Figure 9, which verifies the effectiveness of the fusion strategy. In step 2, the weight distribution of the contrast between the sliding window center and the edge region, as shown in Figure 10a, is introduced to decrease the target diffusion energy and reduce the false alarm probability. On this basis, the exponential weighted likelihood ratio is modeled in step 3 to construct the multi-source fusion detection factor, which is indicated in Figure 10b. In step 4, the second-order statistic is deduced to achieve the CFAR threshold. One can see from Figure 11 that the proposed LRWB detection method could further improve the detection performance. Besides the self-transmitting and self-receiving operation mode, the LRWB-detection method is available for other operation modes. The reasons are chiefly as follows, for different configurations, the echoes with multiple satellites can be combined in the Cartesian coordinate based on the projection relationship, where the target signals corresponding to different satellites are presented as distinct iso-range lines.

Compared with the recent work (LRB detection method) [4], the proposed method achieves a significant multi-source fusion detection performance based on LEO constellation, which is verified from the experimental results.

5. Conclusions

The existing theoretical research on multi-source fusion detection mainly focuses on the incoherent energy accumulation in image domain, which does not deeply explore the difference between the target cell and other background cells caused by the high-speed movement of LEO satellite platform. Therefore, it is necessary to explore and construct a novel fusion detection theory based on LEO-based satellite constellation. In this paper, the proposed multi-source fusion CFAR detection method is carried out from two aspects, i.e., SCR and SNR. On one hand, the distribution characteristic difference between the target and the scene clutter in DFR domain is applied to realize the clutter suppression effectively. On the other hand, the precise focusing of multi-source echo is completed by introducing the pre-compensation function. On this basis, the exponential weighted

likelihood ratio model is deduced in terms of the given multi-source fusion CFAR detection theory to further improve the target SNR. Simulation results indicate that the proposed method provides an efficient way for moving target detection with regard of LEO-based satellite constellation. Our future work will concentrate on exploring the fusion method among different types of satellite echoes, including communication, navigation and radar, and thus to expand the universality of multi-source fusion detection theory.

Author Contributions: Conceptualization, C.D., Y.L. and W.W.; methodology, C.D. and Y.L.; software, C.D., Y.L. and W.W.; validation, W.W. and J.L.; formal analysis, C.D.; investigation, C.D. and Y.L.; resources, C.D. and Y.L.; data curation, C.D. and Y.L.; writing—original draft preparation, C.D.; writing—review and editing, Y.L. and W.W.; visualization, Y.L. and J.L.; supervision, J.L.; project administration, Y.L. and J.L.; funding acquisition, Y.L. All authors have read and agreed to the published version of the manuscript.

Funding: This research was funded by National Natural Science Foundation of China, grant number 62107033.

Acknowledgments: The authors are grateful to University of Electronic Science and Technology of China for supporting this research. We also thank the associate editor and anonymous reviewers for their insightful comments and suggestions.

Conflicts of Interest: The authors declare no conflict of interest.

References

1. Tregloan-Reed, J.; Otarola, A.; Unda-Sanzana, E.; Haeussler, B.; Gaete, F.; Colque, J.P.; González-Fernández, C.; Anais, J.; Molina, V.; González, R.; et al. Optical-to-NIR magnitude measurements of the Starlink LEO Darksat satellite and effectiveness of the darkening treatment. *Astron. Astrophys.* **2014**, *647*, A54. [[CrossRef](#)]
2. Cabot, F.; Anterrieu, E.; Amiot, T.; Kerr, Y.H. ULID: An Unconnected L-band Interferometer Demonstrator. In Proceedings of the 2019 IEEE International Geoscience and Remote Sensing Symposium, Yokohama, Japan, 28 July–2 August 2019.
3. Tonissen, S.D.; Evans, R.J. Target tracking using dynamic programming: Algorithm and performance. In Proceedings of the IEEE Conference on Decision and Control, New Orleans, LA, USA, 13–15 December 1995.
4. Li, Y.; Huang, P.; Lin, C.; Liu, Y. Multi-objective GMTI-TBD technology based on dynamic programming. *J. Electron. Inf. Technol.* **2016**, *37*, 356–363.
5. Du, X.Y.; Hu, W.D.; Wang, C.; Yu, W.X. Technique of resolution matching processing for the fusion detection with narrow-band radars. *J. Signal Process.* **2006**, *22*, 625–629.
6. Wang, Y. Research on Signal Level Fusion Detection Algorithm of Shore Based to Sea Multi Radar. Master's Thesis, Hangzhou Dianzi University, Hangzhou, China, 2017.
7. Zhang, L. Multi Station Detection Sequence Planning and Design of Distributed Radar. Master's Thesis, Xidian University, Xi'an, China, 2018.
8. Hu, Q.; Su, H.; Zhou, S.; Liu, Z. Double threshold CFAR detection algorithm in multistatic radar. *J. Electron. Inf.* **2017**, *7*, 2430–2436.
9. Daniyan, A.; Aldowesh, A.; Gong, Y.; Lambotaran, S. Data association using game theory for multi-target tracking in passive bistatic radar. *Inst. Electr. Electron. Eng. Inc.* **2017**, *13*, 0042–0046.
10. Huang, C.; Li, Z.; Wu, J.; Huang, Y.; Yang, H.; Yang, J. Multistatic Beidou-Based Passive Radar for Maritime Moving Target Detection and Localization. In Proceedings of the 2019 IEEE International Geoscience and Remote Sensing Symposium, Yokohama, Japan, 28 July–2 August 2019.
11. Chen, J.; Zhang, J.; Jin, Y.; Yu, H.; Liang, B.; Yang, D.G. Real-Time Processing of Spaceborne SAR Data With Nonlinear Trajectory Based on Variable PRF. *IEEE Trans. Geosci. Remote Sens.* **2021**, *99*, 1–12. [[CrossRef](#)]
12. Xiong, Y.; Liang, B.; Yu, H.; Chen, J.; Jin, Y.; Xing, M. Processing of Bistatic SAR Data with Nonlinear Trajectory Using A Controlled-SVD Algorithm. *IEEE J. Sel. Top. Appl. Earth Obs. Remote Sens.* **2021**, *1*, 99. [[CrossRef](#)]
13. Li, Y.; Lin, C.; Huang, P. Focus Improvement of Highly Squint Bistatic SAR Based on Nonlinear Chirp Scaling. *IET Radar Sonar Navig.* **2016**, *11*, 171–176. [[CrossRef](#)]
14. Tian, M.; Yang, Z.; Dang, H.; Xu, H.; Huang, P. A Two-Step Detector Based on Point Spread Function Feature for Multi-channel SAR-GMTI Radar. In Proceedings of the 2016 CIE International Conference on Radar, Guangzhou, China, 10–12 October 2016.
15. He, Y.; Guan, J.; Meng, X.W. *Radar Target Detection and CFAR Processing*, 2nd ed.; Tsinghua University Press: Beijing, China, 2011; pp. 9–12.